

Evidence of a resonant structure in the $e^+e^- \rightarrow \pi^+D^0D^{*-}$ cross section between 4.05 and 4.60 GeV

M. Ablikim¹, M. N. Achasov^{9,d}, S. Ahmed¹⁴, M. Albrecht⁴, A. Amoroso^{53A,53C}, F. F. An¹, Q. An^{50,40}, J. Z. Bai¹, Y. Bai³⁹, O. Bakina²⁴, R. Baldini Ferroli^{20A}, Y. Ban³², D. W. Bennett¹⁹, J. V. Bennett⁵, N. Berger²³, M. Bertani^{20A}, D. Bettoni^{21A}, J. M. Bian⁴⁷, F. Bianchi^{53A,53C}, E. Boger^{24,b}, I. Boyko²⁴, R. A. Briere⁵, H. Cai⁵⁵, X. Cai^{1,40}, O. Cakir^{43A}, A. Calcaterra^{20A}, G. F. Cao^{1,44}, S. A. Cetin^{43B}, J. Chai^{53C}, J. F. Chang^{1,40}, G. Chelkov^{24,b,c}, G. Chen¹, H. S. Chen^{1,44}, J. C. Chen¹, M. L. Chen^{1,40}, P. L. Chen⁵¹, S. J. Chen³⁰, X. R. Chen²⁷, Y. B. Chen^{1,40}, X. K. Chu³², G. Cibinetto^{21A}, H. L. Dai^{1,40}, J. P. Dai^{35,h}, A. Dbeyssi¹⁴, D. Dedovich²⁴, Z. Y. Deng¹, A. Denig²³, I. Denysenko²⁴, M. Destefanis^{53A,53C}, F. De Mori^{53A,53C}, Y. Ding²⁸, C. Dong³¹, J. Dong^{1,40}, L. Y. Dong^{1,44}, M. Y. Dong^{1,40,44}, Z. L. Dou³⁰, S. X. Du⁵⁷, P. F. Duan¹, J. Fang^{1,40}, S. S. Fang^{1,44}, Y. Fang¹, R. Farinelli^{21A,21B}, L. Fava^{53B,53C}, S. Fegan²³, F. Feldbauer²³, G. Felici^{20A}, C. Q. Feng^{50,40}, E. Fioravanti^{21A}, M. Fritsch^{23,14}, C. D. Fu¹, Q. Gao¹, X. L. Gao^{50,40}, Y. Gao⁴², Y. G. Gao⁶, Z. Gao^{50,40}, I. Garzia^{21A}, K. Goetzen¹⁰, L. Gong³¹, W. X. Gong^{1,40}, W. Gradl²³, M. Greco^{53A,53C}, M. H. Gu^{1,40}, Y. T. Gu¹², A. Q. Guo¹, R. P. Guo^{1,44}, Y. P. Guo²³, Z. Haddadi²⁶, S. Han⁵⁵, X. Q. Hao¹⁵, F. A. Harris⁴⁵, K. L. He^{1,44}, X. Q. He⁴⁹, F. H. Heinsius⁴, T. Held⁴, Y. K. Heng^{1,40,44}, T. Holtmann⁴, Z. L. Hou¹, H. M. Hu^{1,44}, T. Hu^{1,40,44}, Y. Hu¹, G. S. Huang^{50,40}, J. S. Huang¹⁵, X. T. Huang³⁴, X. Z. Huang³⁰, Z. L. Huang²⁸, T. Hussain⁵², W. Ikegami Andersson⁵⁴, Q. Ji¹, Q. P. Ji¹⁵, X. B. Ji^{1,44}, X. L. Ji^{1,40}, X. S. Jiang^{1,40,44}, X. Y. Jiang³¹, J. B. Jiao³⁴, Z. Jiao¹⁷, D. P. Jin^{1,40,44}, S. Jin^{1,44}, Y. Jin⁴⁶, T. Johansson⁵⁴, A. Julin⁴⁷, N. Kalantar-Nayestanaki²⁶, X. L. Kang¹, X. S. Kang³¹, M. Kavatsyuk²⁶, B. C. Ke⁵, T. Khan^{50,40}, A. Khoukaz⁴⁸, P. Kiese²³, R. Kliemt¹⁰, L. Koch²⁵, O. B. Kolcu^{43B,f}, B. Kopf⁴, M. Kornicer⁵⁰, M. Kuemmel⁴, M. Kuessner⁴, M. Kuhlmann⁴, A. Kupsc⁵⁴, W. Kühn²⁵, J. S. Lange²⁵, M. Lara¹⁹, P. Larin¹⁴, L. Lavezzi^{53C}, H. Leithoff²³, C. Leng^{53C}, C. Li⁵⁴, Cheng Li^{50,40}, D. M. Li⁵⁷, F. Li^{1,40}, F. Y. Li³², G. Li¹, H. B. Li^{1,44}, H. J. Li^{1,44}, J. C. Li¹, Jin Li³³, K. J. Li⁴¹, Kang Li¹³, Ke Li³⁴, Lei Li³, P. L. Li^{50,40}, P. R. Li^{44,7}, Q. Y. Li³⁴, W. D. Li^{1,44}, W. G. Li¹, X. L. Li³⁴, X. N. Li^{1,40}, X. Q. Li³¹, Z. B. Li⁴¹, H. Liang^{50,40}, Y. F. Liang³⁷, Y. T. Liang²⁵, G. R. Liao¹¹, D. X. Lin¹⁴, B. Liu^{35,h}, B. J. Liu¹, C. X. Liu¹, D. Liu^{50,40}, F. H. Liu³⁶, Fang Liu¹, Feng Liu⁶, H. B. Liu¹², H. M. Liu^{1,44}, Huanhuan Liu¹, Huihui Liu¹⁶, J. B. Liu^{50,40}, J. P. Liu⁵⁵, J. Y. Liu^{1,44}, K. Liu⁴², K. Y. Liu²⁸, Ke Liu⁶, L. D. Liu³², P. L. Liu^{1,40}, Q. Liu⁴⁴, S. B. Liu^{50,40}, X. Liu²⁷, Y. B. Liu³¹, Z. A. Liu^{1,40,44}, Zhiqing Liu²³, Y. F. Long³², X. C. Lou^{1,40,44}, H. J. Lu¹⁷, J. G. Lu^{1,40}, Y. Lu¹, Y. P. Lu^{1,40}, C. L. Luo²⁹, M. X. Luo⁵⁶, X. L. Luo^{1,40}, X. R. Lyu⁴⁴, F. C. Ma²⁸, H. L. Ma¹, L. L. Ma³⁴, M. M. Ma^{1,44}, Q. M. Ma¹, T. Ma¹, X. N. Ma³¹, X. Y. Ma^{1,40}, Y. M. Ma³⁴, F. E. Maas¹⁴, M. Maggiora^{53A,53C}, Q. A. Malik⁵², Y. J. Mao³², Z. P. Mao¹, S. Marcello^{53A,53C}, Z. X. Meng⁴⁶, J. G. Messchendorp²⁶, G. Mezzadri^{21B}, J. Min^{1,40}, T. J. Min¹, R. E. Mitchell¹⁹, X. H. Mo^{1,40,44}, Y. J. Mo⁶, C. Morales Morales¹⁴, N. Yu. Muchnoi^{9,d}, H. Muramatsu⁴⁷, A. Mustafa⁴, Y. Nefedov²⁴, F. Nerling¹⁰, I. B. Nikolaev^{9,d}, Z. Ning^{1,40}, S. Nisar⁸, S. L. Niu^{1,40}, X. Y. Niu^{1,44}, S. L. Olsen^{33,j}, Q. Ouyang^{1,40,44}, S. Pacetti^{20B}, Y. Pan^{50,40}, M. Papenbrock⁵⁴, P. Patteri^{20A}, M. Pelizaeus⁴, J. Pellegrino^{53A,53C}, H. P. Peng^{50,40}, K. Peters^{10,g}, J. Pettersson⁵⁴, J. L. Ping²⁹, R. G. Ping^{1,44}, A. Pitka²³, R. Poling⁴⁷, V. Prasad^{50,40}, H. R. Qi², M. Qi³⁰, S. Qian^{1,40}, C. F. Qiao⁴⁴, N. Qin⁵⁵, X. S. Qin⁴, Z. H. Qin^{1,40}, J. F. Qiu¹, K. H. Rashid^{52,i}, C. F. Redmer²³, M. Richter⁴, M. Ripka²³, M. Rolo^{53C}, G. Rong^{1,44}, Ch. Rosner¹⁴, A. Sarantsev^{24,e}, M. Savrie^{21B}, C. Schnier⁴, K. Schoenning⁵⁴, W. Shan³², M. Shao^{50,40}, C. P. Shen², P. X. Shen³¹, X. Y. Shen^{1,44}, H. Y. Sheng¹, J. J. Song³⁴, W. M. Song³⁴, X. Y. Song¹, S. Sosio^{53A,53C}, C. Sowa⁴, S. Spataro^{53A,53C}, G. X. Sun¹, J. F. Sun¹⁵, L. Sun⁵⁵, S. S. Sun^{1,44}, X. H. Sun¹, Y. J. Sun^{50,40}, Y. K. Sun^{50,40}, Y. Z. Sun¹, Z. J. Sun^{1,40}, Z. T. Sun¹⁹, C. J. Tang³⁷, G. Y. Tang¹, X. Tang¹, I. Tapan^{43C}, M. Tiemens²⁶, B. Tsednee²², I. Uman^{43D}, G. S. Varner⁴⁵, B. Wang¹, B. L. Wang⁴⁴, D. Wang³², D. Y. Wang³², Dan Wang⁴⁴, K. Wang^{1,40}, L. L. Wang¹, L. S. Wang¹, M. Wang³⁴, Meng Wang^{1,44}, P. Wang¹, P. L. Wang¹, W. P. Wang^{50,40}, X. F. Wang⁴², Y. Wang³⁸, Y. D. Wang¹⁴, Y. F. Wang^{1,40,44}, Y. Q. Wang²³, Z. Wang^{1,40}, Z. G. Wang^{1,40}, Z. Y. Wang¹, Zongyuan Wang^{1,44}, T. Weber²³, D. H. Wei¹¹, P. Weidenkaff²³, S. P. Wen¹, U. Wiedner⁴, M. Wolke⁵⁴, L. H. Wu¹, L. J. Wu^{1,44}, Z. Wu^{1,40}, L. Xia^{50,40}, Y. Xia¹⁸, D. Xiao¹, H. Xiao⁵¹, Y. J. Xiao^{1,44}, Z. J. Xiao²⁹, Y. G. Xie^{1,40}, Y. H. Xie⁶, X. A. Xiong^{1,44}, Q. L. Xiu^{1,40}, G. F. Xu¹, J. J. Xu^{1,44}, L. Xu¹, Q. J. Xu¹³, Q. N. Xu⁴⁴, X. P. Xu³⁸, L. Yan^{53A,53C}, W. B. Yan^{50,40}, W. C. Yan², Y. H. Yan¹⁸, H. J. Yang^{35,h}, H. X. Yang¹, L. Yang⁵⁵, Y. H. Yang³⁰, Y. X. Yang¹¹, M. Ye^{1,40}, M. H. Ye⁷, J. H. Yin¹, Z. Y. You⁴¹, B. X. Yu^{1,40,44}, C. X. Yu³¹, J. S. Yu²⁷, C. Z. Yuan^{1,44}, Y. Yuan¹, A. Yuncu^{43B,a}, A. A. Zafar⁵², Y. Zeng¹⁸, Z. Zeng^{50,40}, B. X. Zhang¹, B. Y. Zhang^{1,40}, C. C. Zhang¹, D. H. Zhang¹, H. H. Zhang⁴¹, H. Y. Zhang^{1,40}, J. Zhang^{1,44}, J. L. Zhang¹, J. Q. Zhang¹, J. W. Zhang^{1,40,44}, J. Y. Zhang¹, J. Z. Zhang^{1,44}, K. Zhang^{1,44}, L. Zhang⁴², S. Q. Zhang³¹, X. Y. Zhang³⁴, Y. H. Zhang^{1,40}, Y. T. Zhang^{50,40}, Yang Zhang¹, Yao Zhang¹, Yu Zhang⁴⁴, Z. H. Zhang⁶, Z. P. Zhang⁵⁰, Z. Y. Zhang⁵⁵, G. Zhao¹, J. W. Zhao^{1,40}, J. Y. Zhao^{1,44}, J. Z. Zhao^{1,40}, Lei Zhao^{50,40}, Ling Zhao¹, M. G. Zhao³¹, Q. Zhao¹, S. J. Zhao⁵⁷, T. C. Zhao¹, Y. B. Zhao^{1,40}, Z. G. Zhao^{50,40}, A. Zhemchugov^{24,b}, B. Zheng⁵¹, J. P. Zheng^{1,40}, W. J. Zheng³⁴, Y. H. Zheng⁴⁴, B. Zhong²⁹, L. Zhou^{1,40}, X. Zhou⁵⁵, X. K. Zhou^{50,40}, X. R. Zhou^{50,40}, X. Y. Zhou¹, J. Zhu³¹, J. Zhu⁴¹, K. Zhu¹, K. J. Zhu^{1,40,44}, S. Zhu¹, S. H. Zhu⁴⁹, X. L. Zhu⁴², Y. C. Zhu^{50,40}, Y. S. Zhu^{1,44}, Z. A. Zhu^{1,44}, J. Zhuang^{1,40}, B. S. Zou¹, J. H. Zou¹

(BESIII Collaboration)

¹ Institute of High Energy Physics, Beijing 100049, People's Republic of China² Beihang University, Beijing 100191, People's Republic of China³ Beijing Institute of Petrochemical Technology, Beijing 102617, People's Republic of China⁴ Bochum Ruhr-University, D-44780 Bochum, Germany⁵ Carnegie Mellon University, Pittsburgh, Pennsylvania 15213, USA⁶ Central China Normal University, Wuhan 430079, People's Republic of China⁷ China Center of Advanced Science and Technology, Beijing 100190, People's Republic of China⁸ COMSATS Institute of Information Technology, Lahore, Defence Road, Off Raiwind Road, 54000 Lahore, Pakistan

- ⁹ *G.I. Budker Institute of Nuclear Physics SB RAS (BINP), Novosibirsk 630090, Russia*
- ¹⁰ *GSI Helmholtzcentre for Heavy Ion Research GmbH, D-64291 Darmstadt, Germany*
- ¹¹ *Guangxi Normal University, Guilin 541004, People's Republic of China*
- ¹² *Guangxi University, Nanning 530004, People's Republic of China*
- ¹³ *Hangzhou Normal University, Hangzhou 310036, People's Republic of China*
- ¹⁴ *Helmholtz Institute Mainz, Johann-Joachim-Becher-Weg 45, D-55099 Mainz, Germany*
- ¹⁵ *Henan Normal University, Xinxiang 453007, People's Republic of China*
- ¹⁶ *Henan University of Science and Technology, Luoyang 471003, People's Republic of China*
- ¹⁷ *Huangshan College, Huangshan 245000, People's Republic of China*
- ¹⁸ *Human University, Changsha 410082, People's Republic of China*
- ¹⁹ *Indiana University, Bloomington, Indiana 47405, USA*
- ²⁰ *(A)INFN Laboratori Nazionali di Frascati, I-00044, Frascati, Italy; (B)INFN and University of Perugia, I-06100, Perugia, Italy*
- ²¹ *(A)INFN Sezione di Ferrara, I-44122, Ferrara, Italy; (B)University of Ferrara, I-44122, Ferrara, Italy*
- ²² *Institute of Physics and Technology, Peace Ave. 54B, Ulaanbaatar 13330, Mongolia*
- ²³ *Johannes Gutenberg University of Mainz, Johann-Joachim-Becher-Weg 45, D-55099 Mainz, Germany*
- ²⁴ *Joint Institute for Nuclear Research, 141980 Dubna, Moscow region, Russia*
- ²⁵ *Justus-Liebig-Universitaet Giessen, II. Physikalisches Institut, Heinrich-Buff-Ring 16, D-35392 Giessen, Germany*
- ²⁶ *KVI-CART, University of Groningen, NL-9747 AA Groningen, The Netherlands*
- ²⁷ *Lanzhou University, Lanzhou 730000, People's Republic of China*
- ²⁸ *Liaoning University, Shenyang 110036, People's Republic of China*
- ²⁹ *Nanjing Normal University, Nanjing 210023, People's Republic of China*
- ³⁰ *Nanjing University, Nanjing 210093, People's Republic of China*
- ³¹ *Nankai University, Tianjin 300071, People's Republic of China*
- ³² *Peking University, Beijing 100871, People's Republic of China*
- ³³ *Seoul National University, Seoul, 151-747 Korea*
- ³⁴ *Shandong University, Jinan 250100, People's Republic of China*
- ³⁵ *Shanghai Jiao Tong University, Shanghai 200240, People's Republic of China*
- ³⁶ *Shanxi University, Taiyuan 030006, People's Republic of China*
- ³⁷ *Sichuan University, Chengdu 610064, People's Republic of China*
- ³⁸ *Soochow University, Suzhou 215006, People's Republic of China*
- ³⁹ *Southeast University, Nanjing 211100, People's Republic of China*
- ⁴⁰ *State Key Laboratory of Particle Detection and Electronics, Beijing 100049, Hefei 230026, People's Republic of China*
- ⁴¹ *Sun Yat-Sen University, Guangzhou 510275, People's Republic of China*
- ⁴² *Tsinghua University, Beijing 100084, People's Republic of China*
- ⁴³ *(A)Ankara University, 06100 Tandogan, Ankara, Turkey; (B)Istanbul Bilgi University, 34060 Eyup, Istanbul, Turkey; (C)Uludag University, 16059 Bursa, Turkey; (D)Near East University, Nicosia, North Cyprus, Mersin 10, Turkey*
- ⁴⁴ *University of Chinese Academy of Sciences, Beijing 100049, People's Republic of China*
- ⁴⁵ *University of Hawaii, Honolulu, Hawaii 96822, USA*
- ⁴⁶ *University of Jinan, Jinan 250022, People's Republic of China*
- ⁴⁷ *University of Minnesota, Minneapolis, Minnesota 55455, USA*
- ⁴⁸ *University of Muenster, Wilhelm-Klemm-Str. 9, 48149 Muenster, Germany*
- ⁴⁹ *University of Science and Technology Liaoning, Anshan 114051, People's Republic of China*
- ⁵⁰ *University of Science and Technology of China, Hefei 230026, People's Republic of China*
- ⁵¹ *University of South China, Hengyang 421001, People's Republic of China*
- ⁵² *University of the Punjab, Lahore-54590, Pakistan*
- ⁵³ *(A)University of Turin, I-10125, Turin, Italy; (B)University of Eastern Piedmont, I-15121, Alessandria, Italy; (C)INFN, I-10125, Turin, Italy*
- ⁵⁴ *Uppsala University, Box 516, SE-75120 Uppsala, Sweden*
- ⁵⁵ *Wuhan University, Wuhan 430072, People's Republic of China*
- ⁵⁶ *Zhejiang University, Hangzhou 310027, People's Republic of China*
- ⁵⁷ *Zhengzhou University, Zhengzhou 450001, People's Republic of China*
- ^a *Also at Bogazici University, 34342 Istanbul, Turkey*
- ^b *Also at the Moscow Institute of Physics and Technology, Moscow 141700, Russia*
- ^c *Also at the Functional Electronics Laboratory, Tomsk State University, Tomsk, 634050, Russia*
- ^d *Also at the Novosibirsk State University, Novosibirsk, 630090, Russia*
- ^e *Also at the NRC "Kurchatov Institute", PNPI, 188300, Gatchina, Russia*
- ^f *Also at Istanbul Arel University, 34295 Istanbul, Turkey*
- ^g *Also at Goethe University Frankfurt, 60323 Frankfurt am Main, Germany*
- ^h *Also at Key Laboratory for Particle Physics, Astrophysics and Cosmology, Ministry of Education; Shanghai Key Laboratory for Particle Physics and Cosmology; Institute of Nuclear and Particle Physics, Shanghai 200240, People's Republic of China*
- ⁱ *Government College Women University, Sialkot - 51310. Punjab, Pakistan.*
- ^j *Currently at: Center for Underground Physics, Institute for Basic Science, Daejeon 34126, Korea*

(Dated: June 25, 2019)

The cross section of the process $e^+e^- \rightarrow \pi^+D^0D^{*-}$ for center-of-mass energies from 4.05 to 4.60 GeV is measured precisely using data samples collected with the BESIII detector operating at the BEPCII storage ring. Two enhancements are clearly visible in the cross section around 4.23 and 4.40 GeV. Using several models to describe the dressed cross section yields stable parameters for the first enhancement, which has a mass of $4228.6 \pm 4.1 \pm 5.9$ MeV/ c^2 and a width of $77.1 \pm 6.8 \pm 6.9$ MeV, where the first uncertainties are statistical and the second ones are systematic. Our resonant mass is consistent with previous observations of the $Y(4220)$ state and the theoretical prediction of a $D\bar{D}_1(2420)$ molecule. This result is the first observation of $Y(4220)$ associated with an open-charm final state. Fits with three resonance functions with additional $Y(4260)$, $Y(4320)$, $Y(4360)$, $\psi(4415)$, or a new resonance, do not show significant contributions from either of these resonances. The second enhancement is not from a single known resonance. It could contain contributions from $\psi(4415)$ and other resonances, and a detailed amplitude analysis is required to better understand this enhancement.

PACS numbers: 14.40.Rt, 13.25.Gv, 14.40.Pq, 13.66.Bc

A series of charmonium-like states, $Y(4260)$, $Y(4360)$, and $Y(4660)$, have been observed in e^+e^- annihilation at the *BABAR* [1–4], Belle [5–8] and CLEO-c experiments [9, 10]. These newly-observed Y states exceed the number of vector charmonium states predicted by potential models [11] in this energy region; they are thus good candidates for new types of exotic particles, such as hybrids [12], tetraquarks [13], and hadronic molecules [14]. Many experimental measurements and theoretical interpretations have been proposed for these Y states [15]. Since all Y states thus far have been observed only in hidden-charm processes, yet their masses are close to open-charm thresholds, studies of the open-charm production cross section in e^+e^- annihilation will provide important information on their properties. The *BABAR*, Belle, and CLEO-c experiments have reported numerous measurements of the exclusive open-charm production cross sections [16–18]. However, no evidence for open-charm production of these Y states was found.

As the first observed charmonium-like state with $J^{PC} = 1^{--}$, the $Y(4260)$ has remained a mystery. The cross section for e^+e^- annihilation into $D^{(*)}\bar{D}^{(*)}$ pairs shows a dip at the resonance mass, 4.26 GeV/ c^2 [18]. However, the $Y(4260)$ mass is only about 29 MeV/ c^2 below the nominal threshold for $D\bar{D}_1(2420)$, which is the first open-charm relative S -wave channel coupling to $J^{PC} = 1^{--}$. The $D\bar{D}_1(2420)$ molecule model is proposed as an interpretation of the $Y(4260)$, but it predicts a significantly smaller mass of about 4.22 GeV/ c^2 [19, 20]. Recently, the precise measurement of the production cross section for $e^+e^- \rightarrow \pi^+\pi^-J/\psi$ from the BESIII experiment [21] indicates that the structure around 4260 MeV/ c^2 actually consists of two resonances with masses 4222 MeV/ c^2 and 4320 MeV/ c^2 . The mass of the former resonance (referred to as $Y(4220)$ hereafter) is consistent with the prediction of the $D\bar{D}_1(2420)$ molecule model. Furthermore, a $Y(4220)$ resonance has also been reported by the BESIII collaboration in the cross-section measurements of $e^+e^- \rightarrow \omega\chi_{c0}$ [22], $e^+e^- \rightarrow \pi^+\pi^-h_c$ [23], and $e^+e^- \rightarrow \pi^+\pi^-\psi(3686)$ [24].

In addition, a new resonant structure with mass around 4.39 GeV/ c^2 , the $Y(4390)$, has been reported by BESIII in the reactions $e^+e^- \rightarrow \pi^+\pi^-h_c$ [23] and $e^+e^- \rightarrow \pi^+\pi^-\psi(3686)$ [24]. The mass of the $Y(4390)$ is about 45 MeV/ c^2 and 70 MeV/ c^2 higher than those of the $Y(4360)$ [25] and the second component of the $Y(4260)$ observed in $e^+e^- \rightarrow \pi^+\pi^-J/\psi$ by BESIII [21], respectively. The production of $e^+e^- \rightarrow \pi D\bar{D}^*$ is expected to be strongly enhanced above the nominal $D\bar{D}_1(2420)$ threshold and could be a key for understanding existing puzzles with these Y states [20].

The cross section of $e^+e^- \rightarrow \pi^+D^0D^{*-}$ was first measured by the Belle experiment using initial-state radiation (ISR) [26]. No evidence for charmonium(-like) states was found within their statistics. In this Letter, we report improved measurements of the production cross section of $e^+e^- \rightarrow \pi^+D^0D^{*-}$ at center-of-mass energies (\sqrt{s}) from 4.05 to 4.60 GeV using data samples taken at 84 energy points [27] with the BESIII detector [28]. The data set contains 15 energy points with integrated luminosities larger than 40 pb $^{-1}$ (“ XYZ data” hereafter), and 69 energy points with integrated luminosities smaller than 20 pb $^{-1}$ (“ R -scan data” hereafter). The D^0 meson is reconstructed in the $D^0 \rightarrow K^-\pi^+$ decay channel. The bachelor π^+ is also reconstructed, while the D^{*-} is not reconstructed directly, but is inferred from energy-momentum conservation. Charge-conjugate modes are implied, unless otherwise noted.

The BESIII detector is described in detail elsewhere [28]. A Monte Carlo (MC) simulation based on GEANT4 [29] includes the geometric description of the BESIII detector and its response. For each energy point, we generate MC samples of the signal process, $e^+e^- \rightarrow \pi^+D^0D^{*-}$, and the isospin partner process, $e^+e^- \rightarrow \pi^+D^-D^{*0}$, according to phase space (PHSP MC). The effect of ISR is simulated with KKMC [30] with a maximum energy for the ISR photon corresponding to the $\pi^+D^0D^{*-}$ mass threshold. Possible background contributions are estimated with KKMC-generated ‘inclusive’ MC samples with integrated luminosities comparable to

the XYZ data, where the known decay modes are simulated with EVTGEN [31] using branching fractions taken from the PDG [25], and the remaining unknown decays are simulated with the LUNDCHARM model [32].

Charged tracks are detected in the main drift chamber (MDC). The polar angle (θ) must satisfy $|\cos\theta| < 0.93$, and the point of closest approach to the interaction point must be less than 10 cm in the beam direction and less than 1 cm in the perpendicular plane. Particle identification (PID) for charged tracks combines the measurements of the energy loss dE/dx in the MDC and the flight time information from scintillation counters and forms a likelihood $\mathcal{L}(h)$ for each hadron ($h = \pi, K$) hypothesis. A track is identified as K (π) when $\mathcal{L}(K) > \mathcal{L}(\pi)$ ($\mathcal{L}(\pi) > \mathcal{L}(K)$). The selected charged tracks are used to reconstruct D^0 meson candidates from $K^-\pi^+$ track pairs. If there is more than one D^0 candidate in an event, we choose the one whose invariant mass $M(K^-\pi^+)$ is closest to the world-average D^0 mass, $m(D^0)$ [25]. The signal region is defined as $|M(K^-\pi^+) - m(D^0)| < 15 \text{ MeV}/c^2$. To select the bachelor π^+ , at least one extra charged track, which is not used in the D^0 candidate and has charge opposite to that of the reconstructed K^- , is chosen with the same selection criteria as described above. The $e^+e^- \rightarrow D^*\bar{D}^*$ background events are rejected by vetoing any $D^0\pi^+$ candidates satisfying $M(D^0\pi^+) < 2.03 \text{ GeV}/c^2$. After the above requirements, the presence of a D^{*-} meson is inferred by the invariant mass recoiling against the $D^0\pi^+$ system, $RM(D^0\pi^+)$. To improve the mass resolution, the corrected recoil mass, $RM_{\text{cor}}(D^0\pi^+) = RM(D^0\pi^+) + M(K^-\pi^+) - m(D^0)$, is used, as shown in Fig. 1. If there is more than one bachelor π^+ in the event, the one whose $RM_{\text{cor}}(D^0\pi^+)$ is closest to the world average D^{*-} mass, $m(D^{*-})$, is selected. A study of the inclusive MC samples shows that only the isospin partner process $e^+e^- \rightarrow \pi^+D^-D^{*0}$ (BKG1, hereafter) has an enhancement around the D^{*-} mass region in the $RM_{\text{cor}}(D^0\pi^+)$ distribution. The shape of this background process is different at each energy point and is taken from the MC simulation. The $RM_{\text{cor}}(D^0\pi^+)$ distribution of the remaining background processes (BKG2, hereafter) does not peak and can be described by a first-order polynomial function.

An unbinned maximum likelihood fit to the $RM_{\text{cor}}(D^0\pi^+)$ distribution is performed to determine the signal yields. The signal shape is derived from the MC shape convolved with a Gaussian function. The background shape is parameterized as a sum of the shape from the PHSP MC sample for BKG1 and a first-order polynomial function for BKG2. We perform a simultaneous fit to the $RM_{\text{cor}}(D^0\pi^+)$ distributions for all data samples to determine the yields of signal and background. The mean values of the Gaussian smearing function are constrained to be the same for all energy points. A center-of-mass energy-dependent width of the Gaussian function is obtained by fitting the widths of

the five high-luminosity ($> 500 \text{ pb}^{-1}$) data samples at $\sqrt{s} = 4.2263, 4.2580, 4.3583, 4.4156, \text{ and } 4.5995 \text{ GeV}$ with a first-order polynomial function, where these five widths are obtained by separate fits to the corresponding $RM_{\text{cor}}(D^0\pi^+)$ distributions. The widths at $\sqrt{s} < 4.2263 \text{ GeV}$ are fixed to that at $\sqrt{s} = 4.2263 \text{ GeV}$, since the fitted widths are close to zero. Figure 1 shows the fit result at $\sqrt{s} = 4.5995 \text{ GeV}$. The signal region is defined as $|RM_{\text{cor}}(D^0\pi^+) - \Delta M - m(D^{*-})| < 20 \text{ MeV}/c^2$, where ΔM is the mean value of the Gaussian function obtained from the fit. A sideband region, used below, is defined as $1.91 < RM_{\text{cor}}(D^0\pi^+) < 1.95 \text{ GeV}/c^2$.

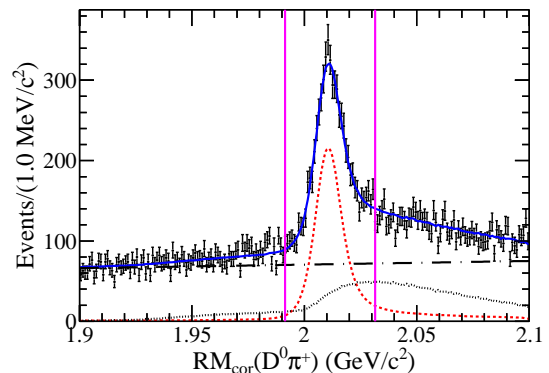


FIG. 1. (Color online) Fit to the distribution of $RM_{\text{cor}}(D^0\pi^+)$ for the data sample at $\sqrt{s} = 4.5995 \text{ GeV}$. The black dots with error bars are data, the solid line (blue) describes the total fit, the dashed line (red) describes the signal shape, the dotted and dash-dotted lines (black) describe BKG1 and BKG2, respectively. The pink vertical lines mark the signal region.

The Born cross sections at the individual energy points are calculated using

$$\sigma^{\text{B}} = \frac{N^{\text{obs}}}{\mathcal{L}(1 + \delta) \frac{1}{|1 - \Pi|^2} \mathcal{B}(D^0 \rightarrow K^-\pi^+) \epsilon}, \quad (1)$$

where N^{obs} is the signal yield, \mathcal{L} is the integrated luminosity [33], $1 + \delta$ is the ISR correction factor [34], $\frac{1}{|1 - \Pi|^2}$ is the correction factor from vacuum polarization [35], $\mathcal{B}(D^0 \rightarrow K^-\pi^+) = (3.93 \pm 0.04)\%$ [25], and ϵ is the detection efficiency. Efficiencies at $\sqrt{s} = 4.2263, 4.2580, 4.3583, 4.4156 \text{ and } 4.5995 \text{ GeV}$ are calculated with MC simulated data samples [36] that are generated by the data-driven BODY3 generator based on EVTGEN [31], taking into account the influence of possible intermediate states ($Z_c(3885)^-$ in the D^0D^{*-} system [37, 38] and highly-excited D states in the π^+D^0 or π^+D^{*-} systems). Since the BODY3 generator requires a large selected sample obtained from events in the signal region after subtracting the background contribution (estimated with the events in the sideband region for BKG2 and MC simulation from BKG1), it is only used for the five energy points with high luminosity. Efficiencies at the other energy points are estimated with PHSP MC samples, with

appropriate uncertainties included later. The obtained Born cross sections, which are consistent with and more precise than those of Belle [26], are summarized in the supplemental material [27] together with all quantities used in their calculation.

The systematic uncertainties in the cross section measurements are listed in Table I. The uncertainty in luminosity is 1.0% at each energy point [39]. The uncertainty in $\mathcal{B}(D^0 \rightarrow K^- \pi^+)$ is 1.0% [25]. The uncertainty in the ISR correction factor is 3.0% [34]. The uncertainties associated with the detection efficiencies include tracking and PID efficiencies (1.0% per track), D^0 and D^{*-} mass window requirements, and signal MC model. The uncertainties associated with the D^0 and D^{*-} mass windows are estimated by repeating the analysis with an altered mass window requirement; the relative changes in the cross sections are taken as systematic uncertainties. The uncertainties associated with the BODY3 signal MC model consist of three parts: the choice of binning, and the BKG1 and BKG2 subtractions. The uncertainty associated with the choice of binning is estimated by repeating the simulation with an altered bin size. The uncertainty associated with the BKG1 subtraction is studied by replacing the PHSP MC sample with MC samples of processes including the intermediate states $e^+e^- \rightarrow \bar{D}_2^*(2460)^0 D^{*0}$, $\bar{D}_2^*(2460)^0 \rightarrow \pi^+ D^-$ and $e^+e^- \rightarrow D_1(2460)^+ D^-$, $D_1(2460)^+ \rightarrow \pi^+ D^{*0}$. For the BKG2 uncertainty, we replace the sideband events with the inclusive MC sample when subtracting the background. The maximum relative changes on the detection efficiency are taken as the corresponding uncertainties. The total signal MC model uncertainty is the sum in quadrature of these three contributions. To estimate the uncertainties of the signal MC model for the low-luminosity data, we estimate the detection efficiencies for the five energy points of large luminosity with the PHSP MC samples; the resultant largest difference with respect to the nominal efficiencies, 5.3%, is assigned as the corresponding uncertainty for the low-luminosity energy points. The uncertainties associated with signal shape, background shape, and fit range in the signal yield extraction are determined by changing the signal shape to the pure MC shape, by changing the background func-

tion from a linear polynomial function to a second-order one, and by changing the fit range, respectively. Due to limited statistics, fit results at the energy points with low luminosity suffer large statistical fluctuations in such fits; thus, the largest systematic uncertainties from the five large luminosity data samples are adopted. Assuming no significant correlations between sources, the total systematic uncertainty is obtained as the sum in quadrature.

The dressed cross section, which includes vacuum polarization effects, is shown in Fig. 2. Two enhancements around 4.23 and 4.40 GeV, denoted hereafter as R_1 and R_2 , are clearly visible. A maximum likelihood

TABLE I. Systematic uncertainties in the measurements of the Born cross sections (%). From the second to sixth columns are the systematic uncertainties of the five high-luminosity energy points while ‘‘Other’’ gives the systematic uncertainties of all other energy points.

\sqrt{s} (GeV)	4.2263	4.2580	4.3583	4.4156	4.5995	Other
Luminosity	1.0	1.0	1.0	1.0	1.0	1.0
$\mathcal{B}(D^0 \rightarrow K^- \pi^+)$	1.0	1.0	1.0	1.0	1.0	1.0
$(1 + \delta)\epsilon$	3.0	3.0	3.0	3.0	3.0	3.0
Tracking	3.0	3.0	3.0	3.0	3.0	3.0
PID	3.0	3.0	3.0	3.0	3.0	3.0
D^0 mass window	0.3	0.1	0.4	0.2	0.7	0.7
D^{*-} mass window	0.2	0.1	0.2	0.3	0.3	0.3
Signal MC model	2.5	2.1	2.9	2.3	2.2	5.3
Signal shape	0.1	1.5	0.8	1.5	2.1	2.1
Background shape	0.4	0.2	0.2	0.1	0.1	0.4
Fit range	0.1	0.2	0.1	0.1	0.1	0.2
Sum in quadrature	6.0	6.0	6.2	6.1	6.2	8.0

fit to the dressed cross section is performed to determine the parameters of these two enhancements. Since the measured cross sections have asymmetric uncertainties for the data with low statistics, the likelihood is described by an asymmetric Gaussian function as discussed in Ref. [23]. In the fit, the total amplitude is described by the coherent sum of a direct three-body phase-space term for $e^+e^- \rightarrow \pi^+ D^0 D^{*-}$ and two relativistic Breit-Wigner (BW) functions, representing the resonant structures R_1 and R_2 :

$$\sigma_{\text{dress}}(m) = \left| c \cdot \sqrt{P(m)} + e^{i\phi_1} B_1(m) \sqrt{P(m)/P(M_1)} + e^{i\phi_2} B_2(m) \sqrt{P(m)/P(M_2)} \right|^2, \quad (2)$$

where the three-body phase-space factor $P(m)$ [25] is modeled as a fixed fourth-order polynomial function.

The factor $B_j(m) = \frac{\sqrt{12\pi\Gamma_j^{\text{el}}\Gamma_j}}{m^2 - M_j^2 + iM_j\Gamma_j}$ with $j = 1$ or 2 is the BW function for a vector state, where $\Gamma_j^{\text{el}} =$

$\Gamma_{e^+e^-} \mathcal{B}(\pi^+ D^0 D^{*-})_j$ is the product of the electronic partial width and the branching fraction to $\pi^+ D^0 D^{*-}$. Parameters c , M_j , Γ_j , Γ_j^{el} , and ϕ_j are the free parameters in the nominal fit. Only statistical uncertainties on the dressed cross sections are considered in the fit. We also

fit the dressed cross section with the coherent sum of one resonance and a phase-space term; the change of the likelihood value, $\Delta(-2\ln L)$, with respect to that of nominal fit including two resonances is 124.3. Taking into account the change in the number of degrees of freedom (4), the statistical significance of the two-resonance model over the one-resonance model is greater than 10σ .

Belle has observed the $\psi(4415)$ in $\psi(4415) \rightarrow D\bar{D}_2^*(2460)$ [40] which can also decay to the final state considered in this analysis. Considering the observations of other charmonium(-like) states, models fixing the mass and width of R_2 to those of $Y(4260)$, $Y(4320)$, $Y(4360)$, or $\psi(4415)$ are also investigated and ruled out with a confidence level equivalent to more than 5.0σ . There are complicated effects in the high mass enhancement which require further detailed amplitude analysis. Models including one additional known resonance, either $Y(4260)$, $Y(4320)$, $Y(4360)$, or $\psi(4415)$, in which the masses and widths of these resonances are fixed to the world average values [25], can improve the fit quality. However, the statistical significances of the additional resonances are only 0.4σ , 0.4σ , 1.4σ , and 1.6σ , respectively. The statistical significance of a fit which includes an additional unknown resonance with free parameters is only 0.8σ , accounting for the two extra free parameters. All above models yield a stable set of parameters for R_1 but wildly varying parameters for R_2 . Conservatively, we only report the resonant parameters of R_1 , which are $M = (4228.6 \pm 4.1 \pm 5.9) \text{ MeV}/c^2$ and $\Gamma = (77.1 \pm 6.8 \pm 6.9) \text{ MeV}$.

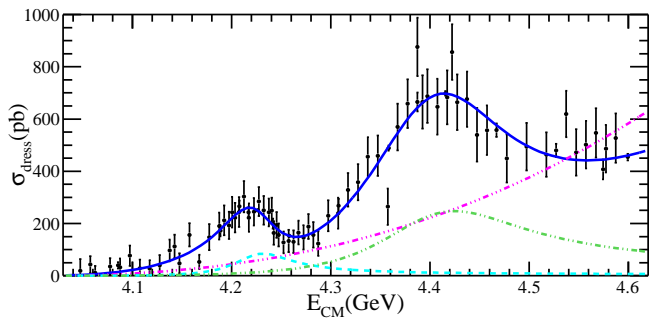


FIG. 2. (Color online) Fit to the dressed cross section of $e^+e^- \rightarrow \pi^+D^0D^{*-}$, where the black dots with error bars are the measured cross sections and the blue line shows the fit result. The error bars are statistical only. The pink dashed triple-dot line describes the phase-space contribution, the green dashed double-dot line describes the R_2 contribution, and the light blue dashed line describes the R_1 contribution.

The systematic uncertainties on the resonance parameters are mainly from the uncertainties of the absolute center-of-mass energy measurements, the beam energy spread, the cross section measurements, and the parameterization of the three-body phase-space factor. The uncertainty of the energy measurement (0.8 MeV) is propagated to the masses of the resonances. To estimate the

uncertainty due to the beam energy spread (1.6 MeV), an alternative fit is performed in which the amplitude described in Eq. 2 is convolved with a Gaussian function whose width is 1.6 MeV, and the resultant differences, 1.2 MeV/ c^2 for the mass and 0.6 MeV for the width of the R_1 resonance, are taken as systematic uncertainties. The uncertainty associated with the cross section measurements consists of two parts. The first is from the common uncertainties of the measured cross sections (tracking, PID, luminosity, and $\mathcal{B}(D^0 \rightarrow K^-\pi^+)$) for all energy points (4.5%); we shift up or down all measured cross sections by 4.5% simultaneously and repeat the fit on the measured cross sections. The differences, 0.1 MeV/ c^2 for the mass and 0.1 MeV for the width, are taken as systematic uncertainties for the R_1 resonance. The second part includes all the other uncertainties of the measured cross sections. We add these uncertainties into the statistical ones in quadrature, and repeat the fit. The resulting differences in resonance parameters, 4.8 MeV/ c^2 for the mass and 2.6 MeV for the width of R_1 , are taken as a systematic uncertainties. The uncertainty associated with the three-body phase-space factor is determined by changing the parameterization function from a fourth-order polynomial function to a third-order one. The resulting differences, 3.1 MeV/ c^2 for the mass and 6.4 MeV for the width, are taken as the corresponding uncertainties for R_1 . Assuming the individual systematic uncertainties are uncorrelated, the total systematic uncertainty is obtained by summing the individual values in quadrature, yielding 5.9 MeV/ c^2 for the mass and 6.9 MeV for the width of R_1 .

In summary, the Born cross section for the process $e^+e^- \rightarrow \pi^+D^0D^{*-}$ is precisely measured using the data samples collected at 84 energy points from 4.05 to 4.60 GeV with the BESIII detector. Two enhancements are observed in the dressed cross sections around 4.23 and 4.40 GeV. Using many models to describe the dressed cross section, we obtain a stable resonant structure around 4.23 GeV, the parameters of which are measured to be $M(R_1) = (4228.6 \pm 4.1 \pm 5.9) \text{ MeV}/c^2$ and $\Gamma(R_1) = (77.1 \pm 6.8 \pm 6.9) \text{ MeV}$, where the first uncertainties are statistical and the second ones systematic. The resonance parameters for the enhancement around 4.40 GeV are strongly dependent on the model assumptions, necessitating further studies.

The statistical significance of the two-resonance model over a one-resonance model is greater than 10σ . This is the first experimental evidence for open-charm production associated with the Y states. The mass of R_1 is consistent with the mass of the resonance observed in $e^+e^- \rightarrow \omega\chi_{c0}$ [22], $e^+e^- \rightarrow \pi^+\pi^-J/\psi$ [21], $e^+e^- \rightarrow \pi^+\pi^-h_c$ [23] and $e^+e^- \rightarrow \pi^+\pi^-\psi(3686)$ [24] by the BESIII experiment as well as the theoretical prediction of the $D\bar{D}_1(2420)$ molecule interpretation [19], while it is lower by about 30 MeV/ c^2 compared to $Y(4260)$ [25]. The width of the first resonance is consistent with that

of $e^+e^- \rightarrow \pi^+\pi^-h_c$ [23] and $e^+e^- \rightarrow \pi^+\pi^-\psi(3686)$ [24], but it is about 39 and 33 MeV/ c^2 higher than that seen in $e^+e^- \rightarrow \omega\chi_{c0}$ [22] and $e^+e^- \rightarrow \pi^+\pi^-J/\psi$ [21], respectively. The measured Born cross section of $e^+e^- \rightarrow \pi^+D^0D^{*-}$ at the $Y(4220)$ peak is higher than the sum of the known hidden-charm channels. Since no other open-charm production associated with this Y state has yet been reported, the $\pi^+D^0D^{*-}$ final state may be the dominant decay mode of the $Y(4220)$ state, as predicted by the $D\bar{D}_1(2420)$ molecule interpretation [19]. No significant contributions from a third resonance are observed using three-resonance models with additional $Y(4260)$, $Y(4320)$, $Y(4360)$, $\psi(4415)$, or a new resonance, while $Y(4320)$ and $\psi(4415)$ are observed in $e^+e^- \rightarrow \pi^+\pi^-J/\psi$ [21] and $\psi(4415) \rightarrow D\bar{D}_2^*(2460)$ [40], respectively. The amplitude studies of this final state and more studies on other open-charm production modes will shed additional light on the nature of these charmonium(-like) states.

The BESIII collaboration thanks the staff of BEPCII and the IHEP computing center for their strong support. This work is supported in part by National Key Basic Research Program of China under Contract No. 2015CB856700; National Natural Science Foundation of China (NSFC) under Contracts Nos. 11521505, 11075174, 11121092, 11235011, 11335008, 11405046, 11425524, 11475185, 11575077, 11605042, 11625523, 11635010; Chinese Academy of Science Focused Science Grant; the Chinese Academy of Sciences (CAS) Large-Scale Scientific Facility Program; the CAS Center for Excellence in Particle Physics (CCEPP); Joint Large-Scale Scientific Facility Funds of the NSFC and CAS under Contracts Nos. U1332201, U1532257, U1504112, U1532258, U1632109; CAS Key Research Program of Frontier Sciences under Contracts Nos. QYZDJ-SSW-SLH003, QYZDJ-SSW-SLH040; 100 Talents Program of CAS; National 1000 Talents Program of China; IN-PAC and Shanghai Key Laboratory for Particle Physics and Cosmology; German Research Foundation DFG under Contracts Nos. Collaborative Research Center CRC 1044, FOR 2359; Istituto Nazionale di Fisica Nucleare, Italy; Koninklijke Nederlandse Akademie van Wetenschappen (KNAW) under Contract No. 530-4CDP03; Ministry of Development of Turkey under Contract No. DPT2006K-120470; National Science and Technology fund; The Swedish Research Council; U. S. Department of Energy under Contracts Nos. DE-FG02-05ER41374, DE-SC-0010118, DE-SC-0010504, DE-SC-0012069; University of Groningen (RuG) and the Helmholtzzentrum fuer Schwerionenforschung GmbH (GSI), Darmstadt; China Postdoctoral Science Foundation.

-
- [1] B. Aubert *et al.* (BABAR Collaboration), Phys. Rev. Lett. **95**, 142001 (2005).
 - [2] B. Aubert *et al.* (BABAR Collaboration), Phys. Rev. Lett. **98**, 212001 (2007).
 - [3] J. P. Lees *et al.* (BABAR Collaboration), Phys. Rev. D **86**, 051102(R) (2012).
 - [4] J. P. Lees *et al.* (BABAR Collaboration), Phys. Rev. D **89**, 111103(R) (2014).
 - [5] X. L. Wang *et al.* (Belle Collaboration), Phys. Rev. Lett. **99**, 142002 (2007).
 - [6] C. Z. Yuan *et al.* (Belle Collaboration), Phys. Rev. Lett. **99**, 182004 (2007).
 - [7] Z. Q. Liu *et al.* (Belle Collaboration), Phys. Rev. Lett. **110**, 252002 (2013).
 - [8] X. L. Wang *et al.* (Belle Collaboration), Phys. Rev. D **91**, 112007 (2015).
 - [9] T. Coan *et al.* (CLEO Collaboration), Phys. Rev. Lett. **96**, 162003 (2006).
 - [10] Q. He *et al.* (CLEO Collaboration), Phys. Rev. D **74**, 091104(R) (2006).
 - [11] E. Eichten *et al.*, Phys. Rev. D **17**, 3090 (1978); **21**, 203 (1980); S. Godfrey and N. Isgur, Phys. Rev. **32**, 189 (1985).
 - [12] S. L. Zhu, Phys. Lett. B **625**, 212 (2005); F. E. Close and P. R. Page, Phys. Lett. B **628**, 215 (2005); E. Kou and O. Pene, Phys. Lett. B **631**, 164 (2005).
 - [13] L. Maiani, V. Riquer, F. Piccinini, and A. D. Polosa, Phys. Rev. D **72**, 031502(R) (2005).
 - [14] X. Liu, X. Q. Zeng, and X. Q. Li, Phys. Rev. D **72**, 054023(R) (2005).
 - [15] H. X. Chen, W. Chen, X. Liu and S. L. Zhu, Phys. Rep. **639**, 1 (2016).
 - [16] B. Aubert *et al.* (BABAR Collaboration), Phys. Rev. D **76**, 111105 (2007).
 - [17] G. Pakhlova *et al.* (Belle Collaboration), Phys. Rev. Lett. **98**, 092001 (2007).
 - [18] D. Cronin-Hennessy *et al.* (CLEO Collaboration), Phys. Rev. D **80**, 072001 (2009).
 - [19] M. Cleven *et al.*, Phys. Rev. D **90**, 074039 (2014).
 - [20] W. Qin, S. R. Xue, and Q. Zhao, Phys. Rev. D **94**, 054035 (2016).
 - [21] M. Ablikim *et al.* (BESIII Collaboration), Phys. Rev. Lett. **118**, 092001 (2017).
 - [22] M. Ablikim *et al.* (BESIII Collaboration), Phys. Rev. Lett. **114**, 092003 (2015).
 - [23] M. Ablikim *et al.* (BESIII Collaboration), Phys. Rev. Lett. **118**, 092002 (2017).
 - [24] M. Ablikim *et al.* (BESIII Collaboration), Phys. Rev. D **96**, 032004 (2017).
 - [25] C. Patrignani *et al.* (Particle Data Group), Chin. Phys. C **40**, 100001 (2016).
 - [26] G. Pakhlova *et al.* (Belle Collaboration), Phys. Rev. D **80**, 091101(R) (2009).
 - [27] See supplemental material at [URL will be inserted by publisher] for a summary of the number of signal events, integrated luminosity, and Born cross section at each energy point.
 - [28] M. Ablikim *et al.* (BESIII Collaboration), Nucl. Instrum. Methods Phys. Res., Sect. A **614**, 345 (2010).
 - [29] S. Agostinelli *et al.* (GEANT4 Collaboration), Nucl. Instrum. Methods Phys. Res., Sect. A **506**, 250 (2003).

- [30] S. Jadach, B. F. L. Ward and Z. Was, *Comp. Phys. Commun.* **130**, 260 (2000); *Phys. Rev. D* **63**, 113009 (2001).
- [31] R. G. Ping, *Chin. Phys. C* **32**, 599 (2008); D. J. Lange, *Nucl. Instrum. Methods Phys. Res., Sect. A* **462**, 152 (2001).
- [32] J. C. Chen, G. S. Huang, X. R. Qi, D. H. Zhang, and Y. S. Zhu, *Phys. Rev. D* **62**, 034003 (2000).
- [33] M. Ablikim *et al.* (BESIII Collaboration), *Chin. Phys. C* **40** (6), 063001 (2016).
- [34] E. A. Kuraev and V. S. Fadin, *Yad. Fiz.* **41**, 733 (1985) [*Sov. J. Nucl. Phys.* **41**, 466 (1985)]. Since the efficiency and the ISR correction depend on the line shape of cross sections, the measured cross sections are used as input and we iterate the procedure until the value of $(1 + \delta)\epsilon$ becomes stable. The largest variation in $(1 + \delta)\epsilon$ during the last two iterations, 3.0%, is taken as the systematic uncertainty.
- [35] S. Actis *et al.*, *Eur. Phys. J. C* **66**, 585 (2010).
- [36] M. Ablikim *et al.* (BESIII Collaboration), *Phys. Rev. D* **89**, 112006 (2014).
- [37] M. Ablikim *et al.* (BESIII Collaboration), *Phys. Rev. Lett.* **112**, 022001 (2014).
- [38] M. Ablikim *et al.* (BESIII Collaboration), *Phys. Rev. D* **92**, 092006 (2015).
- [39] M. Ablikim *et al.* (BESIII Collaboration), *Chin. Phys. C* **39** (9), 093001 (2015).
- [40] G. Pakhlova *et al.* (Belle Collaboration), *Phys. Rev. Lett.* **100**, 062001 (2008).

Supplemental material

The integrated luminosities \mathcal{L} , the numbers of signal events N^{obs} , the ISR correction factors $1 + \delta$, the correction factors from vacuum polarization $\frac{1}{|1-\Pi|^2}$, the detection efficiencies ϵ , and the Born cross sections σ^{B} for XYZ data and R -scan data are summarized in Table II and Table III.

TABLE II. The Born cross sections of $e^+e^- \rightarrow \pi^+D^0D^{*-}$ for XYZ data. The first uncertainties are statistical and the second ones systematic.

\sqrt{s} (GeV)	\mathcal{L} (pb $^{-1}$)	N^{obs}	$1 + \delta$	$\frac{1}{ 1-\Pi ^2}$	ϵ (%)	σ^{B} (pb)
4.0855	52.6	19 \pm 6	0.725	1.06	30.05	40 \pm 13 \pm 3
4.1886	43.1	95 \pm 12	0.749	1.07	41.05	171 \pm 22 \pm 14
4.2077	54.6	190 \pm 16	0.754	1.07	41.73	263 \pm 22 \pm 21
4.2171	54.1	175 $_{-15}^{+16}$	0.765	1.07	41.86	241 $_{-21}^{+22}$ \pm 19
4.2263	1091.7	3885 \pm 72	0.786	1.07	42.82	252 \pm 5 \pm 15
4.2417	55.6	157 $_{-15}^{+16}$	0.858	1.06	39.64	199 $_{-19}^{+20}$ \pm 16
4.2580	825.7	1817 \pm 56	0.903	1.06	38.17	153 \pm 5 \pm 9
4.3079	44.9	162 \pm 16	0.813	1.06	40.11	267 \pm 26 \pm 21
4.3583	539.8	3788 \pm 80	0.787	1.05	43.95	491 \pm 10 \pm 30
4.3874	55.2	510 \pm 28	0.798	1.05	42.01	666 \pm 37 \pm 53
4.4156	1073.6	10899 \pm 142	0.821	1.05	42.76	698 \pm 9 \pm 43
4.4671	109.9	871 $_{-41}^{+42}$	0.887	1.06	38.34	559 $_{-26}^{+27}$ \pm 45
4.5271	110.0	748 $_{-40}^{+41}$	0.931	1.06	36.46	481 $_{-26}^{+26}$ \pm 38
4.5745	47.7	271 $_{-25}^{+26}$	0.925	1.06	36.37	406 $_{-37}^{+39}$ \pm 32
4.5995	566.9	3605 \pm 101	0.916	1.06	36.06	462 \pm 13 \pm 29

TABLE III. The Born cross sections of $e^+e^- \rightarrow \pi^+D^0D^{*-}$ for R -scan data. The first uncertainties are statistical and the second ones systematic.

\sqrt{s} (GeV)	\mathcal{L} (pb $^{-1}$)	N^{obs}	$1 + \delta$	$\frac{1}{ 1-\Pi ^2}$	ϵ (%)	σ^{B} (pb)
4.0474	6.567	0.3 $_{-0.5}^{+1.0}$	0.707	1.05	8.58	18 $_{-33}^{+60}$ \pm 1
4.0524	6.927	-0.02 $_{-0.7}^{+1.2}$	0.713	1.05	12.49	-1.0 $_{-28.6}^{+48.3}$ \pm 0.1
4.0574	6.338	1.3 $_{-0.8}^{+1.2}$	0.712	1.05	16.01	42 $_{-26}^{+40}$ \pm 3
4.0624	7.022	0.5 $_{-0.9}^{+1.2}$	0.712	1.06	19.43	12 $_{-21}^{+31}$ \pm 1
4.0674	7.271	-1.2 $_{-1.2}^{+1.6}$	0.720	1.06	21.63	-25 $_{-26}^{+35}$ \pm 2
4.0774	7.721	2.2 $_{-1.7}^{+2.1}$	0.723	1.06	26.78	36 $_{-32}^{+34}$ \pm 3
4.0874	7.611	2.3 $_{-2.1}^{+2.5}$	0.728	1.06	30.05	33 $_{-31}^{+37}$ \pm 3
4.0974	7.254	5.2 $_{-2.4}^{+2.8}$	0.663	1.06	33.77	77 $_{-36}^{+42}$ \pm 6
4.1074	7.146	2.1 $_{-2.1}^{+2.6}$	0.683	1.05	35.60	29 $_{-30}^{+36}$ \pm 2
4.1174	7.648	2.2 $_{-2.3}^{+2.8}$	0.691	1.06	36.90	28 $_{-29}^{+34}$ \pm 2
4.1274	7.207	3.1 $_{-2.8}^{+3.3}$	0.699	1.06	37.54	40 $_{-36}^{+42}$ \pm 3
4.1374	7.268	7.9 $_{-3.2}^{+3.6}$	0.708	1.06	38.46	96 $_{-39}^{+44}$ \pm 8
4.1424	7.774	10.0 $_{-3.8}^{+4.2}$	0.710	1.06	39.12	111 $_{-42}^{+47}$ \pm 9
4.1474	7.662	4.2 $_{-3.2}^{+3.6}$	0.719	1.06	39.26	47 $_{-35}^{+40}$ \pm 4
4.1574	7.954	14.7 $_{-4.0}^{+4.4}$	0.726	1.06	39.05	156 $_{-42}^{+47}$ \pm 12
4.1674	18.008	11.6 $_{-5.8}^{+6.3}$	0.734	1.06	40.41	52 $_{-26}^{+28}$ \pm 4
4.1774	7.309	13.4 $_{-4.3}^{+4.7}$	0.743	1.06	39.93	148 $_{-47}^{+52}$ \pm 12
4.1874	7.560	18.8 $_{-4.9}^{+5.3}$	0.754	1.07	41.50	190 $_{-49}^{+54}$ \pm 15
4.1924	7.503	20.4 $_{-5.3}^{+5.8}$	0.760	1.07	40.53	210 $_{-55}^{+60}$ \pm 17
4.1974	7.582	19.2 $_{-5.0}^{+5.4}$	0.762	1.07	41.11	192 $_{-50}^{+54}$ \pm 15
4.2004	6.815	21.9 $_{-5.1}^{+5.5}$	0.761	1.07	41.40	243 $_{-56}^{+61}$ \pm 19
4.2034	7.638	22.5 $_{-5.5}^{+6.0}$	0.762	1.07	41.60	222 $_{-54}^{+59}$ \pm 18

Continued on next page

TABLE IV. Table III-continued from previous page.

\sqrt{s} (GeV)	\mathcal{L} (pb $^{-1}$)	N^{obs}	$1 + \delta$	$\frac{1}{ 1-\Pi ^2}$	ϵ (%)	σ^{B} (pb)
4.2074	7.678	$24.4^{+5.9}_{-5.5}$	0.762	1.07	40.99	$242^{+59}_{-55} \pm 19$
4.2124	7.768	$31.2^{+6.0}_{-6.0}$	0.763	1.07	41.52	$302^{+62}_{-58} \pm 24$
4.2174	7.935	$23.2^{+5.9}_{-5.5}$	0.762	1.07	41.18	$222^{+56}_{-52} \pm 18$
4.2224	8.212	$26.8^{+5.9}_{-5.5}$	0.769	1.07	41.12	$246^{+54}_{-51} \pm 20$
4.2274	8.193	$31.1^{+6.3}_{-5.9}$	0.784	1.07	40.61	$284^{+58}_{-54} \pm 23$
4.2324	8.273	$27.8^{+6.3}_{-5.9}$	0.801	1.06	40.08	$250^{+56}_{-53} \pm 20$
4.2374	7.830	$26.1^{+6.0}_{-5.5}$	0.831	1.06	39.45	$243^{+55}_{-52} \pm 19$
4.2404	8.571	$30.2^{+6.3}_{-5.9}$	0.854	1.06	39.53	$250^{+55}_{-48} \pm 20$
4.2424	8.487	$19.6^{+5.6}_{-5.2}$	0.866	1.06	38.92	$164^{+47}_{-43} \pm 13$
4.2454	8.554	$23.6^{+6.3}_{-5.8}$	0.883	1.06	38.69	$193^{+51}_{-48} \pm 15$
4.2474	8.596	$19.3^{+5.7}_{-5.3}$	0.895	1.06	38.56	$156^{+46}_{-43} \pm 12$
4.2524	8.657	$16.2^{+5.6}_{-5.1}$	0.920	1.06	38.49	$127^{+44}_{-40} \pm 10$
4.2574	8.880	$17.5^{+5.9}_{-5.5}$	0.928	1.06	38.29	$133^{+45}_{-42} \pm 11$
4.2624	8.629	$16.3^{+5.7}_{-5.2}$	0.932	1.06	37.40	$130^{+45}_{-42} \pm 10$
4.2674	8.548	$20.1^{+5.9}_{-5.4}$	0.924	1.06	37.35	$164^{+48}_{-44} \pm 13$
4.2724	8.567	$17.9^{+6.0}_{-5.5}$	0.914	1.06	37.64	$146^{+49}_{-45} \pm 12$
4.2774	8.723	$23.4^{+6.1}_{-5.7}$	0.895	1.06	38.27	$189^{+50}_{-46} \pm 15$
4.2824	8.596	$18.8^{+6.2}_{-5.7}$	0.878	1.06	38.45	$156^{+51}_{-47} \pm 12$
4.2874	9.010	$15.3^{+6.2}_{-5.6}$	0.861	1.06	39.00	$122^{+49}_{-45} \pm 10$
4.2974	8.453	$25.9^{+7.0}_{-6.6}$	0.828	1.06	39.18	$228^{+62}_{-58} \pm 18$
4.3074	8.599	$27.3^{+7.0}_{-6.5}$	0.803	1.06	39.82	$239^{+62}_{-57} \pm 19$
4.3174	9.342	$40.8^{+8.3}_{-7.8}$	0.790	1.05	40.82	$327^{+66}_{-62} \pm 26$
4.3274	8.657	$40.8^{+8.1}_{-7.6}$	0.781	1.05	40.87	$358^{+71}_{-67} \pm 29$
4.3374	8.700	$53.2^{+9.0}_{-8.6}$	0.777	1.05	41.80	$456^{+77}_{-73} \pm 36$
4.3474	8.542	$51.4^{+8.9}_{-8.5}$	0.774	1.05	40.91	$460^{+80}_{-76} \pm 37$
4.3574	8.063	$28.5^{+7.8}_{-7.3}$	0.775	1.05	41.84	$264^{+72}_{-67} \pm 21$
4.3674	8.498	$64.6^{+10.5}_{-10.0}$	0.772	1.05	42.02	$567^{+92}_{-88} \pm 45$
4.3774	8.158	$71.2^{+10.3}_{-9.9}$	0.776	1.05	41.24	$659^{+96}_{-92} \pm 53$
4.3874	7.460	$86.3^{+11.4}_{-10.9}$	0.786	1.05	40.70	$874^{+115}_{-111} \pm 70$
4.3924	7.430	$67.0^{+10.5}_{-10.1}$	0.787	1.05	41.68	$665^{+104}_{-100} \pm 53$
4.3974	7.178	$67.8^{+10.4}_{-9.9}$	0.795	1.05	41.68	$689^{+106}_{-101} \pm 55$
4.4074	6.352	$58.0^{+9.8}_{-9.4}$	0.804	1.05	42.14	$650^{+110}_{-105} \pm 52$
4.4174	7.519	$70.2^{+10.9}_{-10.5}$	0.816	1.05	40.38	$683^{+106}_{-102} \pm 55$
4.4224	7.436	$89.1^{+11.4}_{-10.9}$	0.824	1.06	40.72	$860^{+110}_{-106} \pm 69$
4.4274	6.788	$63.0^{+10.3}_{-9.9}$	0.829	1.06	40.39	$668^{+110}_{-105} \pm 53$
4.4374	7.634	$72.6^{+11.7}_{-11.2}$	0.842	1.06	40.23	$674^{+109}_{-104} \pm 54$
4.4474	7.677	$57.5^{+11.3}_{-10.8}$	0.855	1.06	39.29	$536^{+105}_{-101} \pm 43$
4.4574	8.724	$68.5^{+12.0}_{-11.5}$	0.870	1.06	38.98	$555^{+97}_{-93} \pm 44$
4.4774	8.167	$52.1^{+11.0}_{-10.4}$	0.901	1.06	37.84	$449^{+94}_{-90} \pm 36$
4.4974	7.997	$56.3^{+10.7}_{-10.2}$	0.919	1.06	37.26	$494^{+94}_{-90} \pm 40$
4.5174	8.674	$57.0^{+10.8}_{-10.4}$	0.932	1.06	36.46	$464^{+88}_{-84} \pm 37$
4.5374	9.335	$82.4^{+12.2}_{-11.8}$	0.936	1.06	36.62	$619^{+92}_{-89} \pm 49$
4.5474	8.765	$58.0^{+11.3}_{-10.8}$	0.937	1.06	35.94	$472^{+92}_{-88} \pm 38$
4.5574	8.259	$59.0^{+10.9}_{-10.5}$	0.934	1.06	36.40	$505^{+94}_{-90} \pm 40$
4.5674	8.390	$65.5^{+11.6}_{-11.1}$	0.932	1.06	36.62	$549^{+97}_{-93} \pm 44$
4.5774	8.545	$57.2^{+11.0}_{-10.5}$	0.930	1.06	35.49	$487^{+94}_{-90} \pm 39$
4.5874	8.162	$59.6^{+11.0}_{-10.6}$	0.926	1.06	35.84	$528^{+97}_{-94} \pm 42$